

SEPARATED AT BIRTH: THE ORIGIN OF THE PULSARS B2020+28 AND B2021+51 IN THE CYGNUS SUPERBUBBLE

W. H. T. VLEMINGS¹, J. M. CORDES¹, S. CHATTERJEE²
For the Astrophysical Journal

ABSTRACT

High precision astrometric data have enabled us to determine the trajectories through the Galactic potential for a growing number of pulsars. This has resulted in the discovery of a pulsar pair (B2020+28 and B2021+51) that has a common origin in the Cygnus Superbubble or in one of its related OB associations at an epoch which is comparable with the spin-down ages of the pulsars. Analysis of the Galactic orbits indicates that the progenitors of the pulsars had similar masses and were in a binary system, which was disrupted after the second supernova explosion. The implied pulsar birth velocities are consistent with the high velocities of neutron stars in general. The initial spin period of the pulsar that was formed in the second supernova explosion was ~ 200 ms. A further increase in astrometric accuracy will allow us to more tightly constrain the birth velocities and the kick velocities that were imparted by the two respective supernova explosions. Two additional pulsars in the sample of 24 with parallax measurements may also have originated in the Cygnus Superbubble.

Subject headings: astrometry—stars:kinematics—pulsars:individual (PSR B2020+28, PSR B2021+51)

1. INTRODUCTION

The velocity distribution of pulsars has long ago been shown to extend to much larger velocities than those of their progenitors (Gunn & Ostriker 1970). Several possible scenarios have been suggested as causes for high pulsar velocities. These include asymmetry in the birth supernovae (SN) of pulsars (Shklovskii 1970; Dewey & Cordes 1987) and the disruption of binaries by mass-loss from the SN explosion (Blaauw 1961; Gott, Gunn, & Ostriker 1970). Considerable evidence exists that both effects take place. Exactly how an asymmetry in the core collapse of a SN explosion is converted to a kick imparted on the newly formed neutron star (NS) is still unclear; possibilities include hydrodynamic or convective instabilities (Burrows & Hayes 1996; Janka & Müller 1996; Lai & Goldreich 2000) and mechanisms such as asymmetric neutrino emission in the presence of strong magnetic fields (Arras & Lai 1999).

Binarity is particularly common among the early type O and B stars that are expected to produce Type II SN and subsequently NS; approximately 70% of these stars exist in binary systems (Batten 1967). In about 50% of the binaries, both stars are massive enough to become SN; most of these binaries are disrupted when the first SN occurs, while only a small percentage evolves into NS-NS binaries (Bethe & Brown 1998). Until now 6 of such NS-NS binaries have been detected (Burgay et al. 2003).

While most massive star binaries are disrupted at either the first or the second SN, many individual pulsars originate from such binaries. Identification of these pulsars will allow us to put constraints on kick velocities and the amount of asymmetry in the SN explosions.

Previously, several pairs pulsars were hypothesized to come from the same disrupted binary based on their positional information alone (Gott, Gunn, & Ostriker 1970; Wright 1979). Recently, high precision VLBI astrometry has produced accurate measurements of parallaxes and proper motions of about two dozen nearby pulsars, which

¹ Department of Astronomy, Cornell University, Ithaca, NY 14853; wouter@astro.cornell.edu.

² Jansky Fellow, National Radio Astronomy Observatory, P.O. Box O, Socorro, NM 87801.

allows much more accurate tests for pulsar pair identifications. Using the astrometric data, we have analyzed possible trajectories for the pulsars that take into account the Galactic gravitational potential and plausible values of the unknown radial velocities. We find that two of the pulsars (B2020+28 and B2021+51) have Galactic orbits that cross at an epoch consistent with their spin-down ages, which makes them prime candidates for pulsars that have been ejected from the same binary system. In this paper we first discuss the identification of the pulsar pairs and describe the Galactic potential used to calculate the pulsar orbits (§ 2). The results of the orbit calculations are presented in § 3. The birth location of the pulsars and several possible birth scenarios are discussed in § 4, followed by our conclusions in § 5.

2. IDENTIFICATION OF PULSAR PAIRS

The sample of pulsars with high precision astrometric data to date consists of 24 objects, six of which are recycled pulsars. The complete sample is further discussed in Chatterjee et al. (2004, in preparation). First, the trajectories of the 24 pulsars were determined for 3 different radial velocities ($v_r = -300, 0$ and $+300$ km s⁻¹) in the Galactic potential which is discussed below (§ 2.2). We then further examined the Galactic orbits of those pulsar pairs that cross on the plane of the sky at comparable distances and at a similar epoch. From this analysis we find that B2020+28 and B2021+51 are likely candidates for a pulsar pair with a common origin in the Cygnus Superbubble (CSB). Two other pulsars (B1857–26 and B2016+28) in our sample may also have originated from this region.

2.1. B2020+28 and B2021+51 and their Galactic Orbits

The astrometric properties of B2020+28 and B2021+51, which are listed in Table 1, imply transverse velocities of 307 km s⁻¹ and 120 km s⁻¹ for B2020+28 and B2021+51 respectively. The measured period (P), period derivative (\dot{P}) and dispersion measure (DM) are given in Table 2, along with the spin-down age, $\tau_{sd} = P/2\dot{P}$, and the magnetic field strength $B = 3.2 \times 10^{19} \sqrt{P\dot{P}}$, both for a braking index $n = 3$. Neither of the pulsars appears to have

been recycled through accretion in a binary system, as the values for B are consistent with canonical, non-recycled values.

To determine the minimum distance between the pulsar pair at earlier epochs, we performed Monte Carlo simulations of the Galactic pulsar orbits taking into account the astrometric uncertainties and the unknown radial velocities. We assumed a Gaussian probability distribution for the proper motion and parallax measurements, μ_α , μ_δ and π , with standard deviations, σ_{μ_α} , σ_{μ_δ} and σ_π , respectively. The present day absolute positional uncertainty, estimated at 15 mas, corresponds to only 2×10^{-4} pc at 2 kpc distance and is negligible, as the proper motion errors already correspond to a positional uncertainty of ≈ 5 pc when extrapolated backward in time by 1 Myr. The distribution of the radial velocity was determined assuming a two component pulsar birth velocity distribution ($f_{\mathbf{v}_0}$) as determined by Chatterjee et al. (2004, in preparation) and consistent with the work of Cordes & Chernoff (1998) and Arzoumanian, Chernoff & Cordes (2002). The birth velocity PDF was corrected to first order for the propagation through the Galactic potential for a time corresponding to the age τ of the pulsar. This gives the current velocity PDF:

$$f_{\mathbf{v}}(\mathbf{v}_\perp, v_r) = f_{\mathbf{v}}(\mathbf{v}) = f_{\mathbf{v}_0}(\mathbf{v} + \tau \ddot{\mathbf{z}} \hat{\mathbf{z}}) \quad (1)$$

where we have estimated the true age to be equal to the spin-down age, $\tau = \tau_{\text{sd}}$, and where $\ddot{\mathbf{z}}$ is the acceleration due to the Galactic potential in the z -direction perpendicular to the Galactic plane. Note that discrepancy of the true age from the spin-down age are not significant in our analysis, because we restrict our study to young objects and thus the correction due to the acceleration is small. Then, given the transverse velocities, the conditional PDF for the radial velocity is:

$$f_{v_r}(v_r) = \int d\mathbf{v}_\perp f_{\mathbf{v}}(\mathbf{v}_\perp, v_r) f_{\mathbf{v}_\perp}(\mathbf{v}_\perp) \quad (2)$$

where $f_{\mathbf{v}_\perp}(\mathbf{v}_\perp)$ includes the PDFs of the measurement errors in proper motion and parallax. This conditional PDF was then used to randomly select the pulsar radial velocity in each Monte Carlo trial. The conditional PDFs for B2020+28 and B2021+51 are shown in Fig. 4.

The Galactic orbits of the pulsars cross within 10 pc for $\approx 0.15\%$ of our Monte Carlo simulations. The resulting Galactic orbits of B2020+28 and B2021+51 are shown in Fig. 1 and correspond to co-location ~ 1.9 Myr ago. The figure indicates the pulsar trajectories as seen from an observer at rest in the Solar reference frame and includes the Galactocentric motion of the Sun. Only one of the Galactic orbit pairs that results in a minimum separation < 10 pc between the two pulsars is shown. The contours around the common origin position (starred symbol) indicate the 1, 2 and 3σ likelihood contours of the birth location for Galactic orbit solutions which approach 10 pc. The pulsars are seen to traverse the Cygnus Superbubble region (dashed ellipse), which contains several OB associations (see § 4.1). While there are multiple orbit solutions that yield minimum separations < 10 pc and such co-locations can occur by chance for unrelated pairs, we demonstrate below that the probability of co-location is in this case too large to have been caused by chance. Also the choice of

Galactic potential does not significantly alter the results, as the Galactic orbit integration is only ≈ 2 Myr. Even when no Galactic potential is used, a significant number of pulsar orbits reach a minimum separation < 10 pc.

2.2. Galactic Pulsar Orbits

The pulsar orbits were traced back in time through a three component Stäckel potential, which satisfies the most recent estimates of the Milky Way parameters (Famaey & Dejonghe 2003, hereafter FD03). The three components include a thin disk, a thick disk and a halo component. As shown in FD03, a bulge component did not have to be included explicitly, as the resulting three component potential turns out to simulate an effective bulge. In FD03 several combinations of component parameters are shown to satisfy the Milky Way parameters. In our potential we chose the axis ratios $\epsilon = 75.0, 1.5$ and 1.02 , and relative contributions $k = 0.13, 0.01$ and 1.0 for the thin disk, thick disk and halo respectively. The scaling parameters were then adjusted so that our potential predicts the Oort constants $A = 14.19 \text{ km s}^{-1} \text{ kpc}^{-1}$, $B = -11.69 \text{ km s}^{-1} \text{ kpc}^{-1}$ and a circular velocity $v_{\text{circ}} = 219.7 \text{ km s}^{-1}$ at $R_\odot = 8.5$ kpc. Additionally, our potential has a mass density in the solar neighborhood of $\rho_\odot \approx 0.09 \text{ M}_\odot \text{ pc}^{-3}$. These values agree with those obtained in an analysis of Hipparcos data by Feast & Whitelock (1997). The local mass density is also in agreement with $0.06 \text{ M}_\odot \text{ pc}^{-3} < \rho_\odot < 0.12 \text{ M}_\odot \text{ pc}^{-3}$ determined from Hipparcos observations (Crézé et al. 1998; Holmberg & Flynn 2000; Siebert, Bienaymé, & Soubiran 2003). We assume that perturbations of the Galactic orbit due to small scale structure in the potential are negligible, as our integration times are less than a few Myr.

From the astrometric data we determine the position vector in the Galactic reference frame and the velocity \mathbf{v}_\perp in the plane of the sky. The pulsar velocity \mathbf{v}_{psr} is then calculated with a radial velocity taken from the conditional PDF for radial velocity v_r as described above. After correcting the pulsar velocity \mathbf{v}_{psr} for solar motion with respect to the local standard of rest (LSR) \mathbf{v}_{sun} , differential Galactic rotation \mathbf{v}_{DGR} , and the velocity of the LSR \mathbf{v}_{LSR} , the pulsar velocity in the Galactic reference frame is:

$$\mathbf{v}'_{\text{psr}} = \mathbf{v}_{\text{psr}} - \mathbf{v}_{\text{sun}} - \mathbf{v}_{\text{DGR}} - \mathbf{v}_{\text{LSR}}. \quad (3)$$

This velocity is then used to retrace the pulsar orbit in the Galactic potential with a fourth order Runge-Kutta numerical integration method and fixed time steps of 1000 years.

2.3. Identification of pulsar pairs

A positive pair identification is assumed when simulations of the Galactic orbits produce a significant number of solutions where the minimum orbit separation is < 10 pc at a realistic epoch. At the distance to the pulsars discussed here as determined by the parallax measurements, 10 pc correspond to only $\approx 5 \text{ km s}^{-1}$ uncertainty in space velocity during ≈ 2 Myr. As was shown in Hoogerwerf, de Brujne & de Zeeuw (2001), trajectories that cross within a few pc are only a small fraction of all the orbits consistent with the measurement errors. Here we numerically estimate the probability to detect a pulsar pair within 10 pc

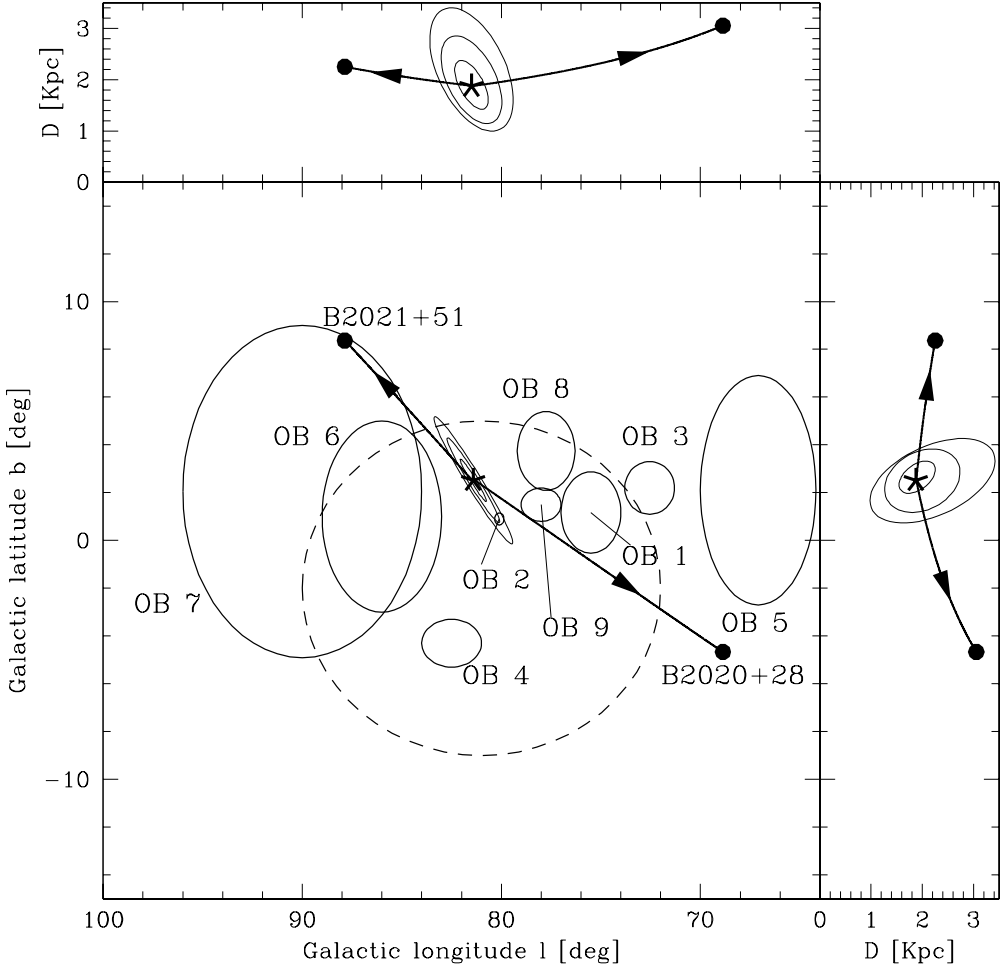


FIG. 1.— The 3-dimensional pulsar motion through the Galactic potential is shown for one of the pulsar orbit solutions that yields a minimum separation < 10 pc (these particular Galactic orbits cross within 4 pc). The dashed circle represents the Cygnus superbubble, while the labeled solid ellipses are the Cygnus OB associations with positions and extents as tabulated by Uyaniker et al. (2001). The extent of OB 2 is unknown and only the center of the association is indicated. The thick solid lines indicate the pulsar paths, with the origin denoted by the starred symbol and the arrows pointing in the direction of motion. The current positions are indicated by the solid dots. The elliptical contours around the pulsars' origin in these panels indicate the 1, 2 and 3σ levels of the likelihood solution for the birth location for Galactic orbit solutions that reach a minimum separation < 10 pc.

of each other when taking into account the measurement uncertainties on the astrometric parameters.

The conditional PDF for the pulsar separation Δ_d at time t is given by:

$$f_{\Delta_d}(\Delta_d | v_{r1}, v_{r2}, \mu_1, \mu_2, \pi_1, \pi_2, t) = \delta(\Delta_d - |\mathbf{x}_{t2} - \mathbf{x}_{t1}|) \quad (4)$$

Here μ_i and π_i are the astrometric data for the two pulsars and v_{ri} is the radial velocity. The separation between the pulsars at time t is:

$$\Delta_d = |\mathbf{x}_{t2} - \mathbf{x}_{t1}|, \quad (5)$$

with

$$\mathbf{x}_t = G(\mathbf{x}, \mathbf{v}, t). \quad (6)$$

The function G describes the trajectory of the pulsar and incorporates the effects of the Galactic potential. In the absence of the Galactic potential $G = \mathbf{x} - \mathbf{v}t$. Eq. 4 is integrated over the astrometric uncertainty PDFs as well as over the radial velocity PDF given by Eq. 2. To obtain the probability for a minimum separation < 10 pc between

the pulsars we integrate further over the separation $\Delta_d < 10$ pc and over the times $t = t_{\min}$ at which this minimum separation occurs,

$$P_c(\tau_0) = \int_{t_{\min}} dt \int_{\Delta_d < 10 \text{ pc}} d\Delta_d f_{d,t}. \quad (7)$$

As t_{\min} depends on the time τ_0 at which the actual minimum separation occurs, the resulting probability function in Eq. 7 is a function of τ_0 that reflects errors that increase as the astrometric properties of the pulsars are projected back in time. Using astrometric errors similar to those determined for B2020+28 and B2021+51, Eq. 7 is evaluated numerically for a pulsar pair that is known to coexist at τ_0 , limiting the analysis to pulsar pairs with $\tau_0 < 10$ Myr. The resulting distribution is shown in Fig. 2a. We find that the probability of finding pulsar orbits that cross within < 10 pc is $P_c(2 \text{ Myr}) \approx 0.16\%$, for a pulsar pair that is known to have a common origin at $\tau_0 = 2$ Myr and that has current day astrometric errors similar to the measure-

TABLE 1
PULSAR ASTROMETRIC DATA

Pulsar	$\alpha_{\text{J}2000.0}$	$\delta_{\text{J}2000.0}$	μ_α (mas yr $^{-1}$)	μ_δ (mas yr $^{-1}$)	π (mas)	D (kpc)
B2020+28	20 22 37.0718	28 54 23.0300	-4.38 ± 0.53	-23.59 ± 0.26	0.37 ± 0.12	$2.7^{+1.3}_{-0.7}$
B2021+51	20 22 49.8655	51 54 50.3881	-5.23 ± 0.17	11.54 ± 0.28	0.50 ± 0.07	$2.0^{+0.3}_{-0.2}$

NOTE.—The data are from Brisken et al. (2002). The positions are at the epoch 2000.0.

TABLE 2
PULSAR CHARACTERISTICS

Pulsar	P (s)	\dot{P} ($\times 10^{-15}$ s s $^{-1}$)	DM (cm $^{-3}$ pc)	τ_{sd} (Myr)	B ($\times 10^{12}$ G)
B2020+28	0.343	1.89	24.62	2.88	0.81
B2021+51	0.529	3.07	22.58	2.75	1.29

ments. This is remarkably consistent with the value of 0.15% found for B2020+28 and B2021+51.

If, instead of being produced in a binary, the pulsar pair crosses at a known minimum distance Δ'_d at time τ_0 , the probability of finding orbits within $\Delta_d < 10$ pc decreases with Δ'_d as shown in Fig. 2b. Here we again used astrometric errors similar to those of B2020+28 and B2021+51, for a pulsar pair that has an actual minimum separation Δ'_d at $\tau_0 = 2$ Myr. Thus, for $\Delta'_d = 0$, the value of $P_c(\Delta'_d = 0) = P_c(\tau_0 = 2 \text{ Myr}) = 0.16\%$. P_c drops sharply for increasing Δ'_d , especially when the astrometric errors in proper motion are decreased. The effect of a reduction of parallax uncertainties is less, as these are generally larger than the several tens of parsec distance scale which was examined for Δ'_d .

To further investigate if the identification of the binary pulsar pair is only a chance coincidence, we simulated 20 samples of nearby (< 3 kpc) pulsars using the birth velocity and scale height distribution as determined by Chatterjee et al. (2004). The samples consisted of 18 pulsars, matching the current sample of non-recycled objects with high precision astrometry. We restricted our simulations to young (< 25 Myr), non-recycled objects. The pulsars were propagated in the Galactic potential to determine their astrometric properties. The radial velocity information was discarded and we determined the closest approach for each of the 153 pulsar pairs in the samples by propagating the pulsars back in time on a grid of possible radial velocities ($|v_r| < 800 \text{ km s}^{-1}$). We found that $\approx 80\%$ of our samples could produce one or more pulsar pairs with a minimum separation < 10 pc. However, the identified pairs are heavily biased toward pulsar ages > 10 Myr. We do not identify any pair younger than 5 Myr. Those pairs that produce the most solutions in this first, coarse, analysis, were then investigated further using the same Monte Carlo method as described in § 2.1. We included uncertainties on the proper motions and parallaxes that were similar to the astrometric uncertainties for B2020+28 and

B2021+51, and the radial velocity was drawn from the actual velocity PDF determined for each pulsar as shown in Eq. 2. We found that the likelihood of finding a minimum separation < 10 pc for these simulated pairs is generally $< 10^{-4}\%$. This low probability rules out any spurious identification as a real related pulsar pair for all of the pulsars in our simulated samples.

However, instead of being a disrupted binary, the pulsars might have originated in one or two of the nearby OB associations, which have enhanced SN rates. Therefore we simulated a large number of pulsars coming from a spherical volume with a radius of approximately 0.8 kpc, which is the volume that encompasses several of the OB associations found in the Cygnus superbubble region (See § 4.1). We simulated 40 pulsars, corresponding to 780 possible pulsar pairs, which is approximately 20% of the number of pulsars estimated to have formed in the CSB (Uyaniker et al. 2001). In an analysis similar to the one performed on our simulated Galactic pulsar samples, we find that approximately 5% of the pulsar pairs can be traced back to within 10 pc for realistic radial velocities. However, in a further analysis of those pairs, we find that the likelihood of a minimum separation < 10 pc is only 0.01%, much less than the likelihood expected for a real pulsar pair. As seen in Fig. 2b, this is consistent with an actual minimum separation of > 40 pc. Thus, we are confident that B2020+28 and B2021+51 are indeed related and originate from the same disrupted binary.

3. ASTROMETRIC PARAMETERS AND AGES OF B2020+28 AND B2021+51

The pulsar pair B2020+28 and B2021+51 was found to have a minimum separation < 10 pc for $\approx 0.15\%$ of 3 million Monte Carlo runs. Here we demonstrate that the values of μ_α , μ_δ and π required for these orbits are typical values allowed by the PDF's for those quantities, and not special values with low probability. Figs. 3 and 4 show the resulting PDFs for the proper motions, paral-

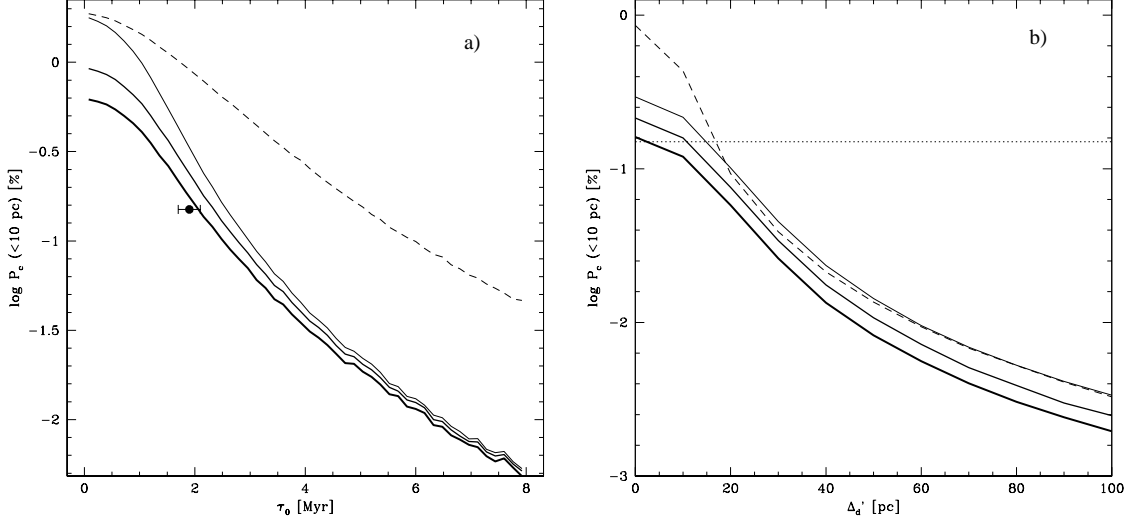


FIG. 2.— The probability function P_c for finding pulsar orbits with a minimum separation < 10 pc. Left panel (a): as a function of the time before the present τ_0 at which the (simulated) pulsars are known to be co-located. For larger τ_0 , the present day proper motions are extrapolated further back in time; the growing errors on the predicted pulsar positions cause the probability of finding pulsar with a minimum separation < 10 pc to decrease. The thick solid line indicates P_c for a pulsar pair with astrometric uncertainties similar to those of B2020+28 and B2021+51. The thinner lines correspond to 30% and 60% improvements on the parallax uncertainties, while the dashed line corresponds to a pulsar pair with uncertainties that are 30% of the μ_α , μ_δ and π uncertainties of B2020+28 and B2021+51. For $\tau_0 > 4$ Myr the curves show some numerical noise. The point indicates the percentage of Galactic orbit solutions with a minimum separation < 10 pc for our observed pulsar pair with the estimated 1σ errors on the determined τ_0 . Right panel (b): as a function of *known* minimum separation at time $\tau_0 = 2$ Myr. The assumed astrometric uncertainties for the four curves are similar to those in the left plot. The horizontal dotted line corresponds to P_c determined for B2020+28 and B2021+51.

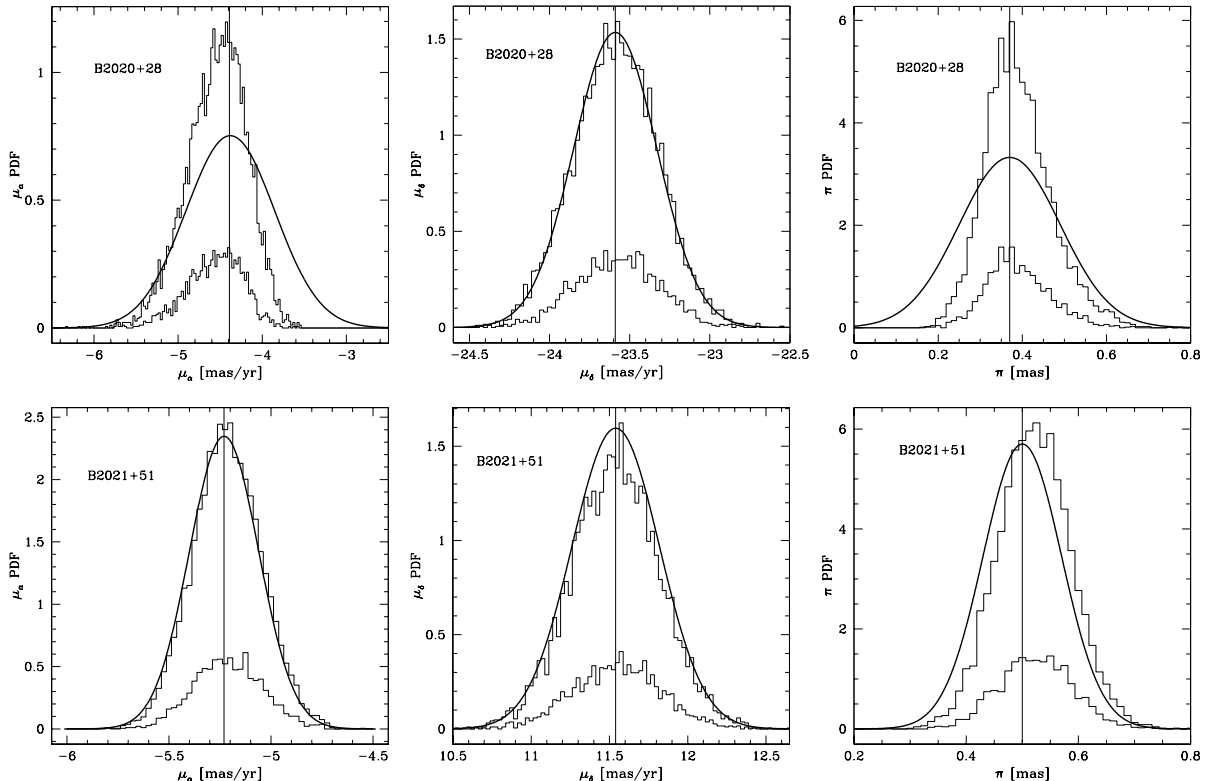


FIG. 3.— Conditional distributions of the astrometric variables μ_α (left), μ_δ (middle) and π (right) for the Galactic orbit solutions that yield minimum separations < 10 pc (thick histogram) and < 5 pc (thin histogram). The top panels are for B2020+28 and the lower panels for B2021+51. The observed values are indicated by the vertical solid lines and the thick solid curve indicate the initial Gaussian PDFs corresponding to the astrometric errors. Note that both histograms are normalized with the same factor.

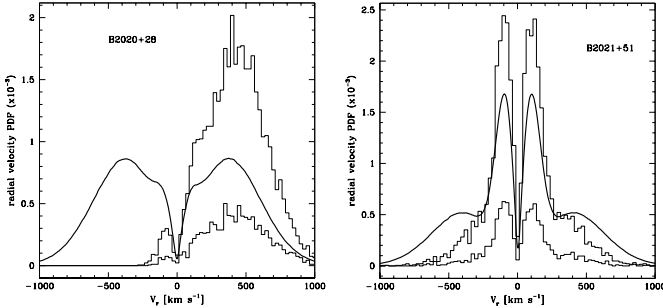


FIG. 4.— Conditional distribution of the radial velocities of B2020+28 (left) and B2021+51 (right) for the Galactic orbit solutions yielding minimum separation < 10 pc (thick histogram) and < 5 pc (thin histogram). The initial conditional PDF for v_r , as described in § 2.1, is indicated by the thick solid curve. The normalization of both histogram is similar.

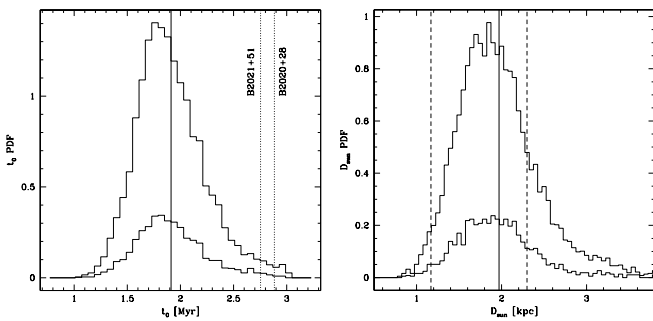


FIG. 5.— Distribution of the times τ_0 (left) and distance to the sun D_{sun} (right) for the Galactic orbit simulation results yielding minimum separations < 10 pc (thick solid) and < 5 pc (thin solid) between B2020+28 and B2021+51. The solid vertical lines denote the mean of the distributions. In the left figure, the dotted vertical lines indicate the spin-down ages of the pulsars. In the right figure, the short dashed vertical lines indicate the estimated distance interval to the Cygnus superbubble and OB associations. The normalization of both histograms is similar.

laxes and radial velocities of the Galactic orbits yielding separations < 10 pc. Also indicated are the distributions for a closest approach of < 5 pc, but we find that the shape of the distribution is not altered significantly. As can be seen, the PDFs for the proper motion of B2021+51 are not significantly different from our input PDFs. The PDF for the parallax of B2021+51 indicates a slight preference for a higher value but this is less than a 0.5σ shift. The orbital solutions that yield close proximity of the two pulsars do not require extreme values for the true proper motion and parallax. For the radial velocity of B2021+51 we find that the distribution of the close Galactic orbits peaks around ± 100 km s $^{-1}$ while higher velocities are unlikely. In the case of B2020+28 the PDF of μ_δ is similar to the initial Gaussian PDF; however, the distribution of μ_α shows a tendency for more negative values and no solutions are found for $\mu_\alpha > -3.5$ mas yr $^{-1}$. Interestingly, the distribution of the parallax of B2020+28 is more confined around the observed value than the observational uncertainties suggest. We can constrain the radial velocity of B2020+28 to be positive. However, a wide range of positive velocities can result in a close encounter between the two pulsars. The B2020+28 radial velocity distribution peaks around 450 km s $^{-1}$. Thus, the astrometric data

for both pulsars are completely consistent with a common origin from a disrupted binary.

We do not find strong correlations between most of the astrometric parameters. The only obvious correlation we find is between π_1 and v_{r_2} , with a larger distance to B2020+28 resulting in a more negative velocity of B2021+51. A modest correlation also exists between μ_{α_1} and π_1 and as a result between μ_{α_1} and v_{r_2} . Future reduction in the astrometric uncertainties will allow us to determine a much tighter relation between v_{r_1} and v_{r_2} .

Fig. 5 shows the distributions of the time of closest approach and the distance to the Sun at that time for the simulations that result in a minimum pulsar separation < 10 pc. We conclude that the binary disrupted approximately 1.9 Myr ago at approximately 1.9 kpc distance from the Sun.

4. THE ORIGIN OF B2020+28 AND B2021+51

4.1. Birth in the Cygnus Superbubble

The CSB is a region with intense radio emission surrounded by soft X-ray emission (Cash et al. 1980). The CSB is approximately 2 Myr old. Uyaniker et al. (2001) estimate that approximately 200 SN have occurred in the CSB within its lifetime, while ~ 1000 SN are needed to power the X-ray emission surrounding the CSB. In fact, Uyaniker et al. argue that the CSB is not a single structure at all, but merely the result from projection effects of several X-ray emitting regions along the line of sight.

As shown in Fig. 1, the CSB region hosts several OB associations at distances between 0.7 and 2.5 kpc. The ages of the OB associations range between 3 and 13 Myr. The distance and location of the pulsar pair at its birth site agrees best with the Cyg OB 2 association at $l = 80.1^\circ$, $b = 0.9^\circ$ and estimated distance $D = 1.44 - 2.10$ kpc, assuming the OB association is at rest with respect to the Sun. Taking a distance of 1.7 kpc (Torres-Dodgen, Carroll, & Tapia 1991), we find that the separation between Cygnus OB 2 and the pulsar pair peaks at approximately 200 pc when the pulsars are at their closest approach, well within the estimated distance interval to OB 2. Cygnus OB 2 is between 3 – 5 Myr old (Torres-Dodgen, Carroll, & Tapia 1991; Uyaniker et al. 2001). It also contains several of the most massive stars ($> 60M_\odot$) in the Galaxy (Abbott, Bieging, & Churchwell 1981; Massey & Thompson 1991). A common origin of the two pulsars in this association ~ 2 Myr ago would require a progenitor binary with two extremely high mass stars ($> 40M_\odot$) with main-sequence lifetimes less than 3 Myr. Such high mass stars are, however, more likely to form black holes or disrupt completely when the SN occurs (Woosley & Weaver 1986). However, a modest velocity of a few times 10 km s $^{-1}$ of the OB associations, could bring some of the older ones in the Cygnus region close to the pulsar pair. Such velocities are quite reasonable, as the peculiar velocities of nearby OB associations are shown to be $\sim 0 - 30$ km s $^{-1}$ (de Zeeuw et al. 1999). Additionally, if the pulsars originated from a binary pair disrupted after the second SN, the first SN can already have imparted a velocity of several tens of km s $^{-1}$. If for instance, the second SN took place 0.5 Myr after the first, this would correspond to a displacement on the sky of almost a degree at the distance of the Cygnus OB associations. Unfortunately, in the absence of accu-

rate velocity information for the Cygnus OB associations, it is impossible to identify the parent association with certainty.

We find that two other pulsars in our sample also cross the area of the CSB for acceptable radial velocities and epochs. Both B1857–26 and B2016+28 passed in the vicinity of the CSB and its OB associations approximately 5 Myr ago. The spin-down ages are 48 and 60 Myr for B1857–26 and B2016+28 respectively. However, their \dot{P} and magnetic fields B are somewhat lower than typical values ($\dot{P} = 2.0$ and 1.5×10^{-16} s s $^{-1}$; $B = 0.35$ and 0.30×10^{-12} Gauss for B1857–26 and B2016+28), indicating that they went through a period of recycling. If so, the differences between their chronological ages and spin-down ages could be large. Therefore, these pulsars could also have been born in the CSB if they originate from binaries that went through an episode of accretion which was interrupted by the second SN.

4.2. Possible birth scenarios

There are several possible scenarios for the common origin of B2020+28 and B2021+51. If they originate from the same binary, the masses of the progenitor stars would likely have been within a few percent of each other to produce two pulsars which have not been recycled and whose properties and spin-down age are so similar. Bethe & Brown (1998) find that 50% of all binaries have stars massive enough to undergo SN. Of these, it is estimated that 2% have masses similar enough that the two SN occur within 1 Myr of each other (Brown 1995). The binary could then have been disrupted after the first SN explosion, with the second SN occurring while the first NS and its companion were already separated. Alternatively, the binary could have survived the first SN only to be disrupted by a second SN a short time afterward. Another possibility is that the pulsars were not part of a binary and our identification is the result of a chance alignment, as discussed earlier (§ 2.3). However, even if the pulsars were not part of a binary, the likelihood analysis in § 2.3 indicates that they both originate from the same OB association in the Cygnus region, within several pc of each other.

Any birth scenario must explain the pulsar velocities at birth, as well as the angle between the pulsar velocity vectors. As shown in Fig. 6, we find that the velocity of B2021+51 at the time of closest approach peaks strongly at ≈ 150 km s $^{-1}$. The velocity of B2020+28 is less well determined, but peaks at ≈ 500 km s $^{-1}$. We find that the distribution of the direction angle, which is the angle between the birth velocity vectors of the pulsars, peaks strongly around 160°.

4.2.1. A binary disrupted after the first SN explosion

Bethe & Brown (1998) estimate that approximately 60% of the binaries are disrupted after the first SN explosion when the kick velocity distribution of Cordes & Chernoff (1998) is used in the analysis. The high space velocities of B2020+28 and B2021+51 should then have been imparted in the first SN explosion, when the progenitor star of the second NS was already well into its red-giant phase. According to the analysis by Tauris & Takens (1998), a kick velocity higher than 600 km s $^{-1}$ would be needed to

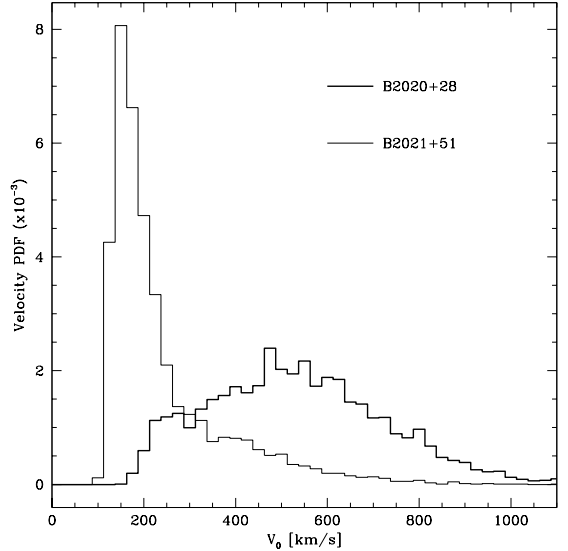


FIG. 6.— The birth velocity distribution of B2020+28 (thick) and B2021+51 (thin) for the Galactic orbit solutions yielding separations of < 10 pc. The birth velocities have been corrected for Galactic rotation.

impart a velocity similar to that of B2021+51; however, the first NS would then be expected to have a velocity of around 700 km s $^{-1}$. Since the velocity of B2020+28 is not very well constrained, we cannot rule out this scenario on the basis of the velocities alone. A somewhat lower kick velocity in the first SN could also explain the high velocities if the second SN (in this case most likely B2021+51) imparted an additional kick. However, as we are able to trace the two pulsars to within a few pc of each other, the second kick must have been in the direction of motion of the runaway pulsar, unless the second SN occurred within a few thousand years when the progenitor star had traveled only a few parsec.

4.2.2. A binary disrupted after the second SN explosion

If the binary survived the first SN explosion, spiral-in and mass-transfer can occur, and the companion star can evolve into a much lighter Helium star with a lifetime of the order of 1 Myr. However, since the pulsars do not exhibit any characteristics of recycling, this is highly unlikely. We thus expect the binary separation to have been large enough so that the two stars evolved independently.

Tauris & Takens (1998) show that for a system with a large binary separation and a high-mass companion, a SN kick of only ~ 200 km s $^{-1}$ can already produce the implied birth velocities that we find for B2020+28 and B2021+51. Using a simple binary model with an initial circular binary orbit we have attempted to reproduce the pulsar velocities and the angle between the birth velocity vectors. If the disruption of the binary was caused only by the (instantaneous) mass-loss in a symmetric SN, the angle between the pulsars' birth velocity vectors cannot be larger than 90° (Gott, Gunn, & Ostriker 1970). However, when we include an asymmetric kick, larger angles can be produced. We find that the model can reproduce the required velocities and direction angle when the companion mass $\sim 9 M_{\odot}$, the binary separation is 2–4 AU

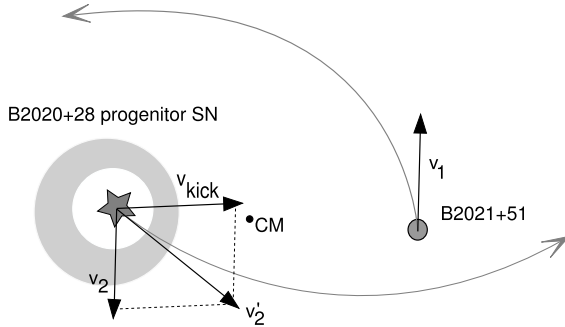


FIG. 7.— Schematic representation of a binary disrupted after the second asymmetric SN explosion (indicated by the starred symbol with the grey annulus) that can produce the observed pulsar pair. The high mass progenitor of the second pulsar (B2020+28) and the NS (B2021+51) have initial circular velocities v_1 and v_2 respectively, around the center of mass (CM). The kick velocity v_{kick} imparted in the second SN is in the direction of the NS companion and the newly created NS moves closely past its companion, resulting in a slingshot effect that contributes to the observed pulsar velocities and their resulting orbits (grey curves).

and the kick velocity is $\approx 200 \text{ km s}^{-1}$ with an angle $\approx 70^\circ$ from the direction of motion of the exploding star toward the companion NS. As the newly created NS moves closely past the first NS, both experience a slingshot effect which accelerates each to the desired velocities. In this simple analysis, we expect B2021+51 to be created in the first SN explosion while B2020+28 was created in the explosion that disrupted the binary system. This scenario is illustrated in Fig. 7.

If the initial binary orbit was elliptical, the orbital position as well as the kick angle must be included in the analysis. It is quite likely that the binary orbit was no longer circular after the first SN had failed to disrupt the system. However, since the circular binary scenario can already easily produce the required velocities and direction angle, an elliptical binary will most likely be able to do the same. Thus, the scenario in which our pulsar pair originates from a binary that was disrupted in the second SN explosion seems the most likely.

5. CONCLUSIONS

After examining the available sample of pulsars that have precision astrometric data, we have found that the pulsars B2020+28 and B2021+51 likely share their origin in a disrupted binary even though they are presently separated by $\sim 23^\circ$ on the plane of the sky. The Galactic orbits of the pulsars, traced back through a 3 component Stäckel potential that satisfies the current Galactic parameters, are found to cross approximately 1.9 Myr ago at 1.9 kpc distance from the Sun in the region known as the Cygnus superbubble. Simulations of pulsar samples, and an analysis of the likelihood functions, show that it is unlikely that our pulsar pair identification is the result from a chance alignment.

The most likely scenario for the creation of the runaway pulsar pair is the disruption of a binary system in the second SN explosion. As no signs of accretion are present, the progenitor stars must have had similar masses and have been in a wide binary orbit. The second SN must

have followed the first by only a short time (< 0.5 Myr). The velocities and direction angle of the pulsars at birth can be explained if the second (asymmetric) SN imparted a kick velocity of $\approx 200 \text{ km s}^{-1}$. The velocity analysis indicates that B2020+28 was created in the second SN.

The system was disrupted ≈ 1.9 Myr ago, which must correspond to the true age of at least one of the pulsars. The spin-down ages of both pulsars are very similar: B2020+28 has a spin-down age of 2.88 Myr, while B2021+51 has a spin-down age of 2.75 Myr. As the relationship of spin-down age to true age is largely uncertain, the similarity between our derived age and the spin-down ages is remarkable. An age of 1.9 Myr implies that the initial period of B2020+28 was 201 ms, assuming a constant braking index of $n = 3$. If the SN that created B2021+51 was the source of the binary disruption, the initial pulsar period will have been 295 ms, also assuming a constant $n = 3$. In both cases, a constant braking index of $n > 4$ can be ruled out.

The most likely three dimensional space velocities of the pulsars at birth are $\approx 150 \text{ km s}^{-1}$ for B2021+51 and $\approx 500 \text{ km s}^{-1}$ for B2020+28. Recent analyses of pulsar velocities have found that a two component birth velocity distribution seems to best fit the current data (Cordes & Chernoff 1998; Arzoumanian, Chernoff & Cordes 2002). Using the sample of pulsars with accurate astrometric data, Chatterjee et al. (2004) find that the pulsar velocities are best described by a 2-component birth velocity distribution with characteristic velocities of 86 km s^{-1} (70%) and 292 km s^{-1} (30%). The probability of finding pulsars with a three dimensional space velocity $\geq 500 \text{ km s}^{-1}$ ranges from $\sim 10\%$ using the Chatterjee et al. (2004) distribution, which has probable selection effects against the highest velocity pulsars, to $\sim 45\%$ for the Arzoumanian, Chernoff & Cordes (2002) distribution, which was based on a much larger sample of pulsars, but used a different methodology that was based largely on DM-distances using the Taylor & Cordes (1993) model. The birth velocities determined for B2020+28 and B2021+51 then indicate that B2021+51, likely created in the first SN explosion, is part of the lower velocity population, while B2020+28, created in the SN explosion that disrupted the binary system, is part of the high velocity component.

The current astrometric data are completely consistent with the common binary origin of the two pulsars and an improvement of astrometric precision is unlikely to invalidate our conclusions. However, as the accuracies of the proper motion and parallax measurements are increased, we will be able to more precisely determine the current radial velocities of the pulsars. This will lead to a significant improvement on the determination of the birth velocities and as a result, we will be able to obtain better constraints for the kick velocities of the SN explosions as well as other characteristics of the progenitor binary system.

As the sample of pulsars with accurate proper motions and parallaxes increases, the identification of additional related pulsar pairs will allow us to put constraints on kick velocities and the amount of asymmetry in the SN explosions. Unfortunately, due to pulsar beaming, we can only detect approximately one out of five pulsars. This ratio is somewhat better for young pulsars, which, as seen in § 2.3, are also the pulsars for which a positive pair identification is the most likely. For a compete sample of nearby, young

pulsars with precision astrometric data, we expect to be able to identify related pulsars for at least 10% of them.

The National Radio Astronomy Observatory is a facility of the National Science Foundation (NSF) operated under cooperative agreement by Associated Universities, Inc. This work at Cornell was supported in part by NSF grants AST 9819931 and AST 0206036.

REFERENCES

Abbott, D. C., Biegling, J. H., & Churchwell, E. 1981, *ApJ*, 250, 645
 Arras, P. & Lai, D. 1999, *ApJ*, 519, 745
 Arzoumanian, Z., Chernoff, D. F. & Cordes, J. M. 2002, *ApJ*, 568, 289
 Batten, A. H. 1967, *ARA&A*, 5, 25
 Bethe, H. A. & Brown, G. E., 1998, *ApJ*, 506, 780
 Blaauw, A. 1961, *Bull. Astron. Inst. Netherlands*, 15, 265
 Brisken, W. F., Benson, J. M., Goss, W. M., & Thorsett, S. E. 2002, *ApJ*, 571, 906
 Brown, G. E. 1995, *ApJ*, 440, 270
 Burgay, M. et al. 2003, *Nature*, 426, 531
 Burrows, A. & Hayes, J. 1996, *Physical Review Letters*, 76, 352
 Cash, W., Charles, P., Bowyer, S., Walter, F., Garmire, G., & Riegler, G. 1980, *ApJ*, 238, L71
 Cordes, J. M. & Chernoff, D. F. 1998, *ApJ*, 505, 315
 Crézé, M., Chereul, E., Bienaymé, O., & Pichon, C. 1998, *A&A*, 329, 920
 Dewey, R. J. & Cordes, J. M. 1987, *ApJ*, 321, 780
 de Zeeuw, P. T., Hoogerwerf, R., de Bruijne, J. H. J., Brown, A. G. A., & Blaauw, A. 1999, *AJ*, 117, 354
 Famaey, B. & Dejonghe, H. 2003, *MNRAS*, 340, 752
 Feast, M. & Whitelock, P. 1997, *MNRAS*, 291, 683
 Gott, J. R. I., Gunn, J. E., & Ostriker, J. P. 1970, *ApJ*, 160, L91
 Gunn, J. E. & Ostriker, J. P. 1970, *ApJ*, 160, 979
 Holmberg, J. & Flynn, C. 2000, *MNRAS*, 313, 209
 Hoogerwerf, R., de Bruijne, J. H. J. & de Zeeuw, P. T., 2001, *A&A*, 365, 49
 Janka, H.-T. & Müller, E. 1996, *A&A*, 306, 167
 Lai, D. & Goldreich, P. 2000, *ApJ*, 535, 402
 Massey, P. & Thompson, A. B. 1991, *AJ*, 101, 1408
 Shklovskii, I. S. 1970, *AZh*, 46, 715
 Siebert, A., Bienaymé, O., & Soubiran, C. 2003, *A&A*, 399, 531
 Tauris, T. M. & Takens, R. J. 1998, *A&A*, 330, 1047
 Taylor, J. H. & Cordes, J. M. 1993, *ApJ*, 411, 674
 Torres-Dodgen, A. V., Carroll, M., & Tapia, M. 1991, *MNRAS*, 249, 1
 Uyaniker, B., Fürst, E., Reich, W., Aschenbach, B. & Wielebinski, R. 2001, *A&A*, 371, 675
 Woosley, S. E. & Weaver, Thomas A., 1986, *ARA&A*, 24, 205
 Wright, G. A. E. 1979, *Nature*, 277, 363